ACS OMEGA

http://pubs.acs.org/journal/acsodf

Article

Photonic Curing Enables Ultrarapid Processing of Highly Conducting β-$Cu_{2-\delta}Se$ Printed Thermoelectric Films in Less Than 10 ms

Md Mofasser Mallick,* Leonard Franke, Andres Georg Rösch, Holger Geßwein, Yolita M. Eggeler, and Uli Lemmer*

Cite This: *ACS Omega* 2022, 7, 10695−10700

Read Online

ACCESS | Metrics & More | Article Recommendations | Supporting Information

ABSTRACT: It has been a challenge to obtain high electrical conductivity in inorganic printed thermoelectric (TE) films due to their high interfacial resistance. In this work, we report a facile synthesis process of Cu−Se-based printable ink for screen printing. A highly conducting TE β-$Cu_{2-\delta}Se$ phase forms in the screen-printed Cu−Se-based film through ≤10 ms sintering using photonic-curing technology, minimizing the interfacial resistance. This enables overcoming the major challenges associated with printed thermoelectrics: (a) to obtain the desired phase, (b) to attain high electrical conductivity, and (c) to obtain flexibility. Furthermore, the photonic-curing process reduces the synthesis time of the TE β-$Cu_{2-\delta}Se$ film from several days to a few milliseconds. The sintered film exhibits a remarkably high electrical conductivity of ∼3710 S cm^{-1} with a TE power factor of ∼100 μW m^{-1} K^{-2}. The fast processing and high conductivity of the film could also be potentially useful for different printed electronics applications.

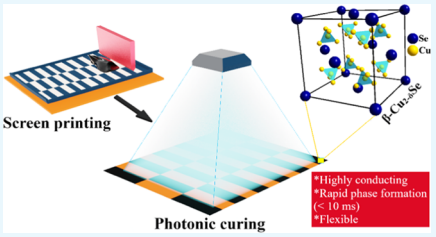

1. INTRODUCTION

In general, different chemical and physical synthesis methods such as arc melting, solid-state reaction melt and growth, mechanical alloying, and hydrothermal synthesis are employed to prepare various thermoelectric (TE) materials.[1] Depending on the type of material, a suitable synthesis method is implemented. The synthesis processes are extremely important; they should be appropriate to get an expected phase and high TE performance. The melt and growth method is widely used to synthesize low-melting-temperature alloys, such as telluride/selenide chalcogenides and Zintl phases. In this process, metal elements with a stoichiometric ratio are kept in a vacuum-sealed quartz tube followed by heating at elevated temperatures for several hours to days so that all of the precursor elements interdiffuse to form the desired phases.[2] The melting points of the metal elements and annealing temperatures are generally determined from the phase diagram of the targeted alloys. The resulting consolidated ingots are ground into a powder and made into pellets using hot-pressing or spark plasma sintering (SPS) to prepare TE components. The mechanical alloying method has also been adopted to synthesize similar TE materials.[3−5] Here, powder elements are mixed in a stoichiometric ratio and ground with a high-energy ball mill for several hours. The milling time and rotation speed of the jar containing balls and the ingredients depend on the formation energies of the alloys to be prepared. The resulting homogeneous milled powder samples are then consolidated into pellets using hot press or SPS. Sometimes, further heat treatment at high temperatures is required to acquire the desirable phase. The Cu_2Se chalcogenide phase is one of the most interesting TE phases for its unique transport properties. The monoclinic α-Cu_2Se is the common phase at room temperature (RT) and transforms into the cubic disordered superionic β-Cu_2Se phase at elevated temperatures. In this phase, two separate sublattices, "Cu" and "Se", build the structure of Cu_2Se. A rigid crystalline symmetric framework is formed by the large Se atoms that help transfer the charge carriers, and the disordered Cu ions diffuse around the Se sublattices, resulting in a strong phonon scattering, facilitating a low lattice thermal conductivity. Therefore, the β-Cu_2Se phase exhibits a liquid-like behavior of the phonons and a crystal-like behavior of the charge carriers, a "phonon-liquid electron-crystal" behavior.[6] Hence, β-Cu_2Se exhibits simultaneously high electrical conductivity and low thermal conductivity. Both the "melt and growth" and mechanical alloying synthesis processes are employed to prepare the bulk Cu_2Se phase, followed by grinding, pressing, and dicing to design Cu_2Se-based bulk TE components. The complete synthesis processes are reported to take up to 10 days.[7−11] Chemical synthesis methods have also been reported to

Received: January 20, 2022
Accepted: February 1, 2022
Published: March 15, 2022

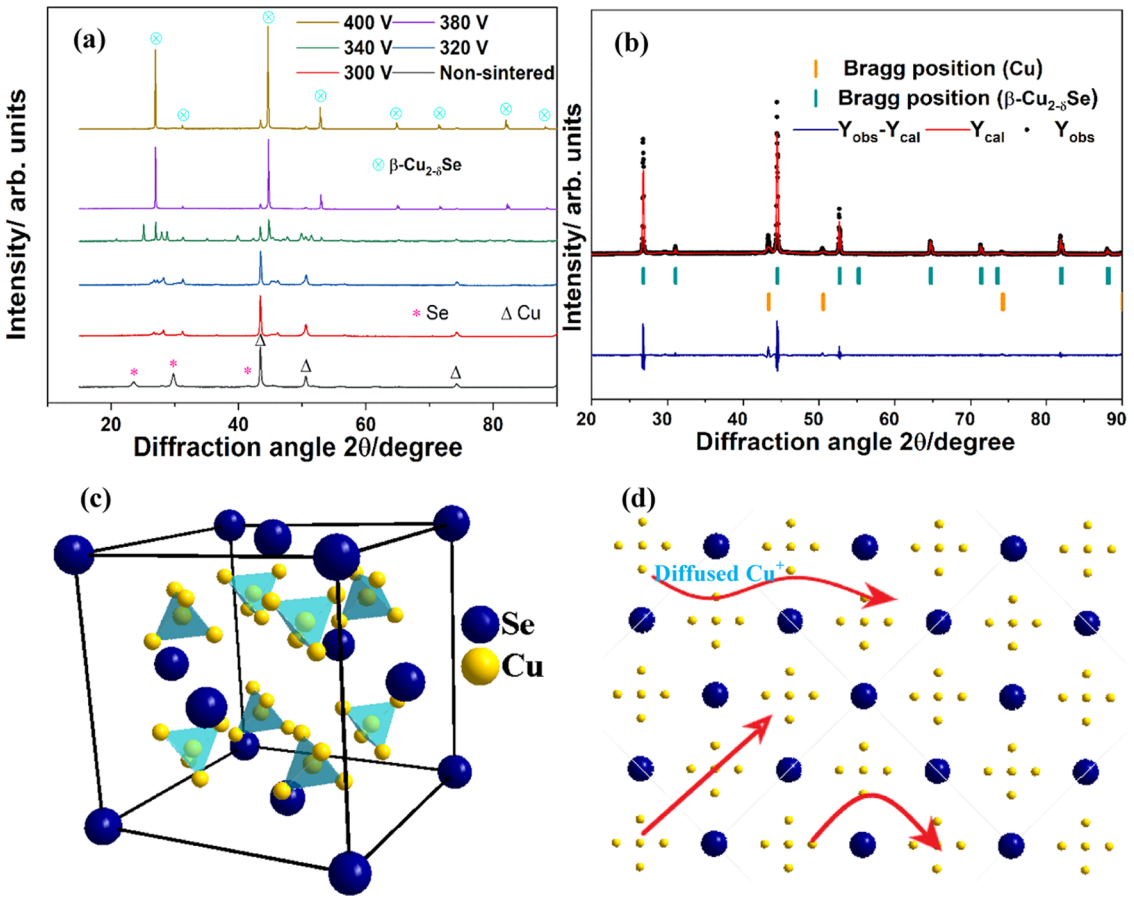

Figure 1. V_P-dependent XRD patterns of the Cu−Se-based printed films at RT (a). Rietveld refinement results of the film for V_P = 380 V (b). β-$Cu_{2-\delta}Se$ is identified as the main phase with a small fraction of unreacted Cu. Unit cell and lattice structure of β-$Cu_{2-\delta}Se$ (c, d).

prepare Cu_2Se, which also involves multiple steps.[12] Apart from a complex and long synthesis process, the Cu_2Se-based bulk TE components reported so far are neither shape-conformal nor flexible. A flexible TE component would potentially be advantageous over its bulk counterparts as this allows wearable and complex geometry applications.[13,14] Hence, efforts have been put forward to synthesize flexible Cu_2Se-based TE films using bulk or chemically prepared Cu_2Se particles.[15,16] Recently, PEDOT:PSS/Cu_2Se-based composite TE films prepared by the vacuum filtration and pressing technique have been reported to exhibit good performance.[17,18] However, unlike printing technology, the synthesis processes of these TE components are not low-cost and involve a set of complex processes.

Recently, we have reported Sb−Bi−Te/β-$Cu_{2-\delta}Se$ TE films prepared by sintering in a vacuum oven. Nevertheless, there is a trade-off between high performance and good flexibility in the films.[19−21] We have also reported high-performance Ag_2Se-based printed n-type TE films prepared by a similar sintering process.[13,22,23] In this work, we have employed a fast photonic-curing technology on printed Cu−Se-based films to address the drawbacks associated with the traditional procedure to fabricate flexible β-$Cu_{2-\delta}Se$-based TE films. We have used screen printing to fabricate TE films with high spatial resolution, and a very fast photonic-curing process is implemented to sinter the films. We have discovered that the TE β-$Cu_{2-\delta}Se$ phase is formed in less than 10 ms in the film, facilitating an ultrahigh electrical conductivity and mechanical flexibility without damaging the low-temperature substrates. The sintering time to form the $Cu_{2-\delta}Se$ phase reduces by 8 orders of magnitude from $\sim 10^6$ s in bulk to $\leq 10^{-2}$ s in the printed film.

2. EXPERIMENTAL METHODS

2.1. Materials. Copper powder (spheroidal) (10−25 μm, 98%, Sigma-Aldrich), Se powder (100 mesh, ≥99.5% trace metal basis, Sigma-Aldrich), *N*-methyl-2-pyrrolidone (NMP) (anhydrous, 99.5%, Sigma-Aldrich), poly(vinylpyrrolidone) (PVP) (average M_w ~40 000, Sigma-Aldrich), and polyethylene naphthalate (PEN) (75 μm, DuPont).

2.2. Synthesis of TE Inks and Films. The Cu−Se-based printable TE ink was prepared using a ball mill, Fritsch Planetary Mill PULVERISETTE 5 premium line. The Cu and Se elemental powders were mixed in a 2:1 atomic ratio in a PVP−NMP (6:94) solution. The blend was then kept in a N2 purged zirconia jar containing 10 mm zirconia balls followed by wet milling for 30 min at 200 rpm. The weight ratio of the balls to the mixture was 10:1. We printed the obtained Cu−Se-based ink on glass and flexible substrates using a semi-automated screen printer ROKUPRINT machine with a screen specification of 600 × 300 90−40 y/22° Hitex. The printed films of the order of 10 μm were dried on a hotplate after printing. After drying at 343 K, the printed films were flash-sintered with 35 μPulses for 8−10 ms, varying the external input flashlamp voltage (V_P) in the range of 300−400 V using a PulseForge 1200 (Novacentrix) photonic-curing machine. The temperatures of the top surface of the printed film, at the interface, and at the bottom of the substrate have been

https://doi.org/10.1021/acsomega.2c00412
ACS Omega 2022, 7, 10695−10700

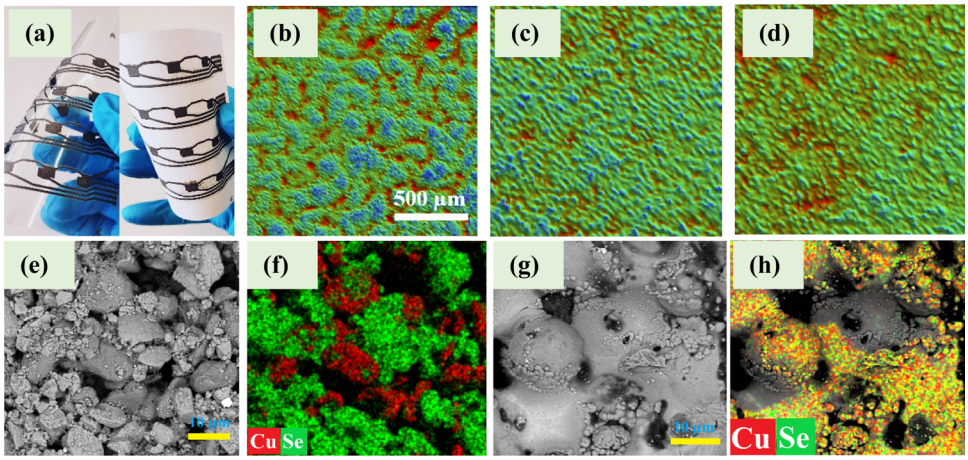

Figure 2. Screen-printed sintered Cu_2Se film on the poly(ethylene terephthalate) (PET) substrate (a). Surface morphologies of the nonsintered film (b), sintered film with V_P = 340 V (c), and sintered film with V_P = 380 V (d) captured by a WLI 3D microscope. The microstructures and elemental maps of the nonsintered film (e, f) and the sintered film with $V_P \geq 340$ V (g, h).

simulated using the interactive numerical model SimPulse for PulseForge photonic-curing tools based on the heat transfer model. It can be seen that the top and interface temperatures reach 973 for V_P = 380 V where the substrate temperature remains near RT (cf. Figure S1). The film temperature decreases below 473 K within 50 ms.

2.3. Characterization Techniques. The phase and crystallographic analyses of the photonic-sintered printed films were conducted using X-ray diffraction (XRD) on a Bruker D8 diffractometer with a Lynxeye XE detector. The temperature-dependent transport parameters of the films were studied using a Hall measurement setup (Linseis HCS 10). The electrical conductivity is determined by the van der paw method with four contacts. A magnetic field is applied perpendicular to the film to produce a Hall voltage (V_H). The Hall coefficient (R_H) is determined from the V_H, which is essential to determine the carrier concentration and mobility. The RT Seebeck coefficient α of the sintered film with V_P = 380 was measured using a custom-built setup. The working principle of the custom-built setup is given in Supporting Information Note 2 of the previous report.[14] The thicknesses and surface morphologies of the printed films were studied by a Bruker 3D microscope based on white-light interferometry (WLI). Microstructural and elemental analyses of the sintered films were conducted using an FEI Quanta 650 environmental scanning electron microscope (ESEM) equipped with a Schottky field emitter and an SSD detector operating with 5 and 15 kV.

3. RESULTS AND DISCUSSION

The crystallographic and phase analyses of the nonsintered and sintered films were extensively studied using the X-ray diffraction (XRD) technique (cf. Figure 1). XRD patterns of the sintered films for different V_P from 300 to 400 V were collected while keeping the sintering time constant at 10 ms. The XRD pattern of the nonsintered printed film corresponds to the two unreacted Cu and Se. The β-$Cu_{2-\delta}Se$ phase starts to grow when V_P reaches 320 V and is found to be fully developed for $V_P \geq 380$ V (cf. Figure 1a). To get insight into the crystallographic structure of the β-$Cu_{2-\delta}Se$ phase, Rietveld refinement of the XRD pattern of the sintered film for V_P = 380 V was performed (cf. Figure 1b). The results indicate that the XRD pattern corresponds to a main cubic β-$Cu_{2-\delta}Se$ phase with space group $Fm\bar{3}m$ and a fraction of unreacted Cu. The nonstoichiometry "δ" is estimated to be up to 0.1. Most probably, the δ is responsible for the RT β-$Cu_{2-\delta}Se$ phase as it is also reported that δ = 0.03 can enable a phase transformation of the conventional α-$Cu_{2-\delta}Se$ phase to the cubic β-Cu_2Se phase. The lattice parameter of the unit cell of the β-$Cu_{2-\delta}Se$ phase is estimated to be a = 5.7(6) Å. The Se atoms in the β-$Cu_{2-\delta}Se$ crystal form a rigid face-centered cubic cell occupying the Wyckoff position 4a (0, 0, 0), and the Cu atoms occupy two different Wyckoff positions 8c (1/4, 1/4, 1/4) and 32f (x, x, x).

The detailed microstructural and morphological analyses of the printed sintered and nonsintered films are included in Figure 2. The screen printability of the Cu−Se-based film was checked using the ROKUPRINT screen-printing machine (cf. Figure 2a). Macroscopic morphologies of the printed Cu_2Se films for sintering and nonsintering conditions were studied using three-dimensional (3D) microscopy; see Figure 2b−d. The morphology of the nonsintered film shows segregated island-like structures of the Cu−Se material. SEM images of the nonsintered and sintered films also show that the film was compacted after sintering with V_P = 380 V and becomes denser (cf. Figure 2e,g). The elemental mapping of the printed films indicates that the Cu and Se elements were segregated in the nonsintered film and they almost fully reacted to form the β-Cu_2Se phase in the sintered film. The b/w regions in the elemental mappings in Figure 2h correspond to the potholes created due to the expulsion of the organic constituents from the film during the sintering process. A sufficient number of data from potholes did not reach the energy-dispersive X-ray analysis (EDX) detector.

The remnant of organic binder PVP could be present in the films; however, it constitutes only 1.6 wt % (<10 vol %) of the films. After sintering, it decomposes releasing <3 vol % of carbon in the film, which is far below the percolation threshold to influence the transport properties.[24] The mechanical flexibility of a 15 mm sintered film for V_P = 380 V has been checked by a semicircular bending test multiple times. The normalized resistance of the film was found to be 1.5 after 10 bending cycles (cf. Figure S2).

3.1. Thermotransport Properties of Photonic-Cured Films. The temperature-dependent transport properties were studied for $V_P \leq 380$ V (cf. Figure 3). The mechanical

https://doi.org/10.1021/acsomega.2c00412
ACS Omega 2022, 7, 10695−10700

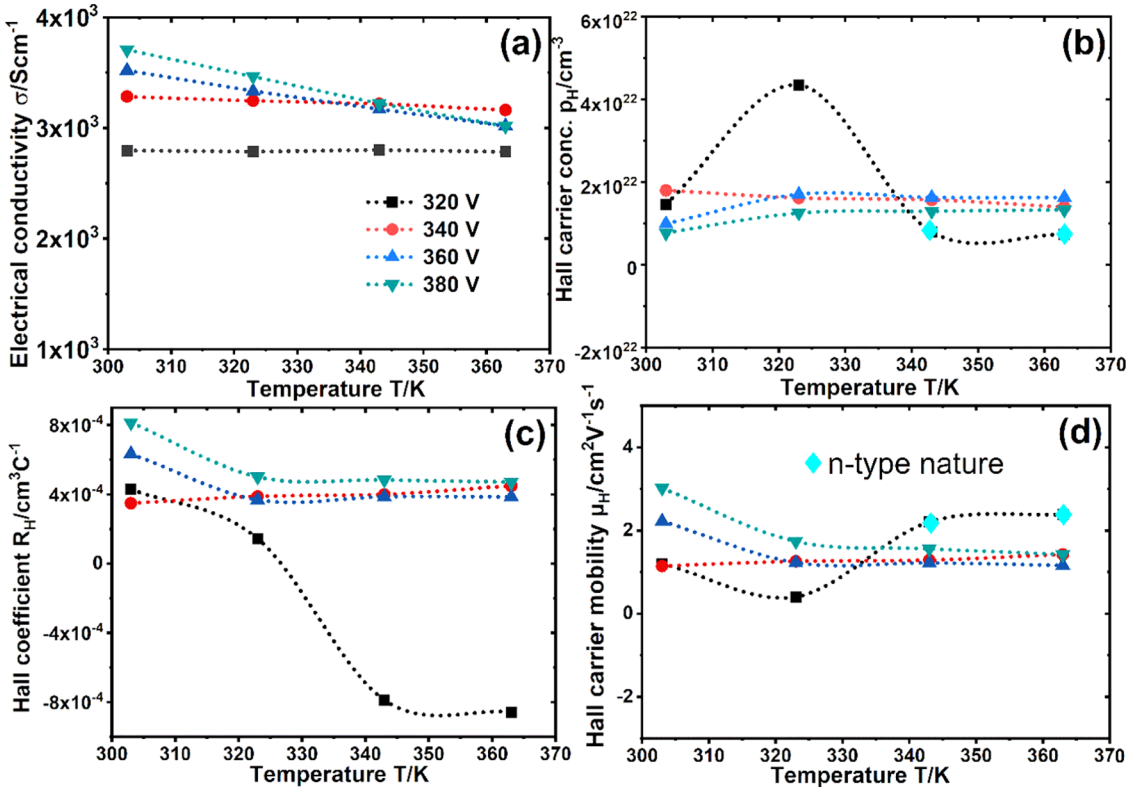

Figure 3. Variation of electrical conductivity σ (a), Hall carrier concentration p_H (b), Hall coefficient R_H (c), and Hall carrier mobility μ_H (d) of the Cu−Se-based printed film with temperature for different V_p, 320 ≤ x ≤ 380.

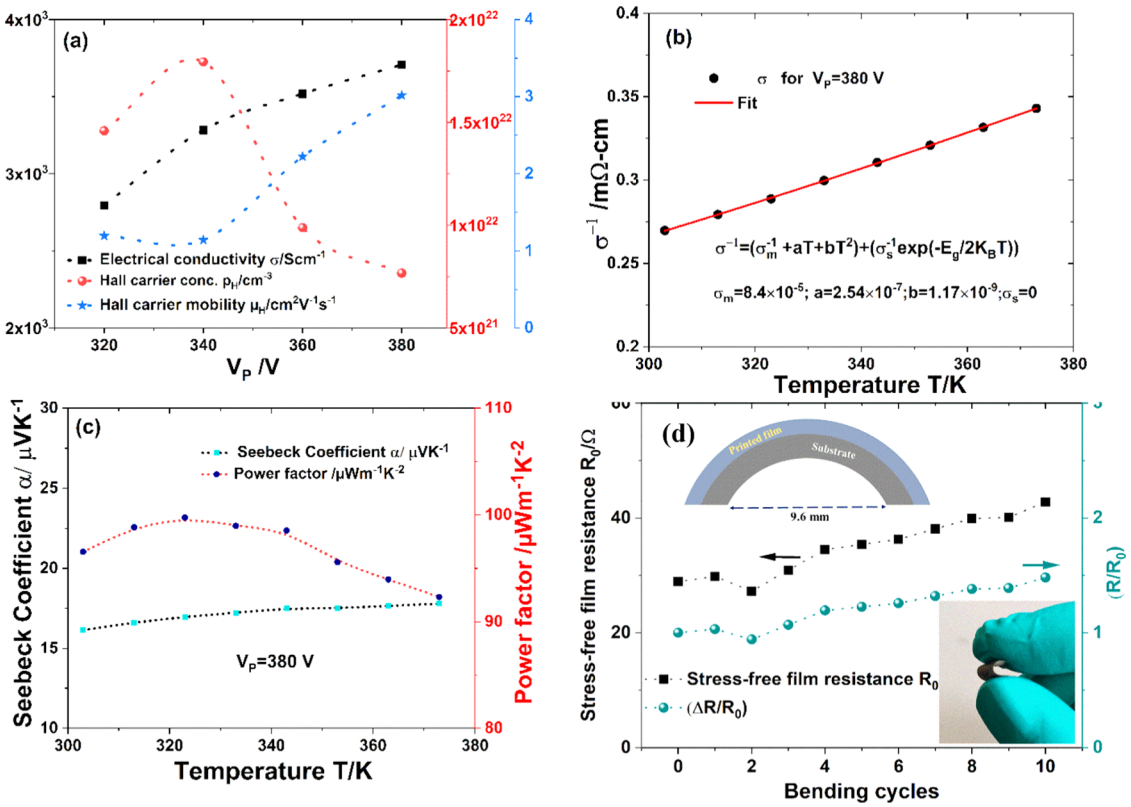

Figure 4. Variation of the transport parameters σ, p_H, and μ_H with the input flashlamp voltage V_P (a). Electric conductivity is modeled, and the line through the data points is a fit (b). Temperature-dependent α and power factor of the photonic-cured film for V_P = 380 V (c). Semicircular bending test of a 15 mm sintered film for V_P = 380 V to check its mechanical flexibility (d).

https://doi.org/10.1021/acsomega.2c00412
ACS Omega 2022, 7, 10695−10700

flexibility and the electrical conductivities σ of the printed film deteriorate for V_P > 380 V. The nonsintered film is found to be insulating and becomes highly conductive after sintering. All of the films show p-type conduction, and the σ increases with increasing V_P, altering the transport properties and the nature of the films for V_P > 340 V (cf. Figure 3a). The negative value of (R_H) at T > 323 K for the film with V_P = 320 V indicates alteration of the conduction nature, from p-type to n-type, as the β-Cu_2Se phase is not formed. Although the Hall carrier concentration (p_H) decreases with increasing V_P, the σ increases because of significant enhancement of the carrier mobility (μ_H) (cf. Figure 3b,d). The films for $V_P \geq$ 360 V show a metallic-like nature, consistent with the previously reported transport phenomena of the pristine β-Cu_2Se-based film.[20]

A surprisingly high σ ~3710 S cm^{-1} is achieved at RT in the flexible printed film for V_P = 380 V. The σ value is much higher than those of most reported Cu_2Se-based bulk materials[6−9] because of leftover unreacted Cu elements in the film. The electrical conductivity σ and Hall mobility μ_H of the printed film increase with increasing the flashlamp voltage V_P, which is directly proportional to the sintering temperature of the film. The insulating organic ingredients in the printed film start to be removed with increasing V_P. The elemental Cu and Se then react to form β-Cu_2Se with further increase of V_P, enhancing the σ of the sintered film (Figure 4). At first, the charge carrier concentration p_H of the film increases with increasing V_P for ≤ 340 V due to the removal of the insulating organic constituents, leaving partially unreacted Cu and Se in the printed film, as shown in Figure 1a.

The amount of the unreacted elements decreases with increasing V_P for V_P > 340 V resulting in the decrease of p_H in the film. As the p_H of the Cu element (~8.55×10^{22} cm^{-3}) is one order of magnitude higher than that for the β-Cu_2Se phase (<5×10^{21} cm^{-3}), with decreasing unreacted Cu, the overall σ decreases for V_P > 340 V. The temperature-dependent electrical transport of the film for V_P = 380 V is modeled using a metal-semiconducting transport equation.[25] The film is found to be metallic in nature (cf. Figure 4b). The RT σ of the sintered film stored in the air atmosphere for V_P = 380 V was measured after many weeks and it is found to be decreased slightly. Storing in an N2 or inert gas environment could prevent decreasing the conductivity. Due to the presence of unreacted Cu elements, the Seebeck coefficient (α) is also found to be lower. A positive α ~16 μV K^{-1} and a TE power factor of ~95 μW m^{-1} K^{-2} are achieved in the film at RT (cf. Figure 4c). The power factor value is twice as high as the previously reported vacuum-sintered β-Cu_2Se film.[20] Unfortunately, we could not determine the thermal conductivity of the film due to the nature of the synthesis process and film specification. However, the thermal conductivity value could be higher compared to the β-Cu_2Se film, resulting in lower ZT due to its high conductivity. In addition to TE applications, the highly conductive p-type β-Cu_2Se film could be potentially employed for printed sensors and optoelectronic applications.[26−28]

4. CONCLUSIONS

A long sintering process at elevated temperatures is one of the most important steps to synthesis a TE phase. However, in printed thermoelectrics, low-temperature substrates with printed precursor materials do not withstand the high-temperature sintering process to form a TE phase. This work employs photonic-curing technology to sinter the printed Cu−Se-based material without damaging the flexible low-temperature substrates. The TE β-Cu_2Se phase is formed within 10 ms through the photonic curing in the printed film. The obtained sintered flexible film exhibits a remarkably high electrical conductivity of 3710 S cm^{-1} with a TE power factor of 95 μW m^{-1} K^{-2} at RT.

■ ASSOCIATED CONTENT

Supporting Information

The Supporting Information is available free of charge at https://pubs.acs.org/doi/10.1021/acsomega.2c00412.

Synthesis of TE inks and films (Supporting Note 1: synthesis methods), numerical model SimPulse for PulseForge photonic-curing tools to determine the film temperature (Figure S1), characterization of the photonic-cured films (Supporting Note 2: characterization techniques), semicircular bending test of the film (Figure S2), and recently reported RT power factor of solution-processed Cu2Se-based flexible films (Table S1) (PDF)

■ AUTHOR INFORMATION

Corresponding Authors

Md Mofasser Mallick − *Light Technology Institute, Karlsruhe Institute of Technology, 76131 Karlsruhe, Germany;* orcid.org/0000-0003-2105-6153; Email: mofasser.mallick@kit.edu

Uli Lemmer − *Light Technology Institute, Karlsruhe Institute of Technology, 76131 Karlsruhe, Germany; Institute of Microstructure Technology, Karlsruhe Institute of Technology, 76344 Eggenstein-Leopoldshafen, Germany;* orcid.org/0000-0001-9892-329X; Email: uli.lemmer@kit.edu

Authors

Leonard Franke − *Light Technology Institute, Karlsruhe Institute of Technology, 76131 Karlsruhe, Germany*

Andres Georg Rösch − *Light Technology Institute, Karlsruhe Institute of Technology, 76131 Karlsruhe, Germany*

Holger Geßwein − *Institute for Applied Materials, Karlsruhe Institute of Technology, 76344 Eggenstein-Leopoldshafen, Germany*

Yolita M. Eggeler − *Laboratory for Electron Microscopy, Karlsruhe Institute of Technology, 76131 Karlsruhe, Germany*

Complete contact information is available at: https://pubs.acs.org/10.1021/acsomega.2c00412

Notes

The authors declare no competing financial interest.

■ ACKNOWLEDGMENTS

The authors acknowledge the Deutsche Forschungsgemeinschaft (DFG, German Research Foundation) under Germany's Excellence Strategy via the Excellence Cluster 3D Matter Made to Order (EXC-2082/1-390761711) for financial support. The authors also acknowledge funding by the Ministry of Science, Research and Arts of the State of Baden Württemberg through the MERAGEM graduate school. The German Federal Environmental Foundation (Deutsche Bundesstiftung Umwelt—DBU) through the DBU Ph.D. scholarship program also supported this work. This project has received funding from

the European Union's Horizon 2020 research and innovation program under grant agreement no. 814945—SolBio-Rev.

REFERENCES

(1) Shi, X. L.; Zou, J.; Chen, Z. G. Advanced Thermoelectric Design: From Materials and Structures to Devices. *Chem. Rev.* **2020**, *120*, 7399−7515.
(2) Li, S.; Li, X.; Ren, Z.; Zhang, Q. Recent Progress towards High Performance of Tin Chalcogenide Thermoelectric Materials. *J. Mater. Chem. A* **2018**, *6*, 2432−2448.
(3) Tewary, A.; Bhatt, R.; Singh, A.; Bhattacharya, S.; Bhatt, P.; Jha, P.; Basu, R.; Sarkar, P.; Muthe, K. P. Tailoring of Thermoelectric Properties in Bi_2Te_3 by Varying the Sintering Temperature. *AIP Conf. Proc.* **2020**, *2265*, No. 030667.
(4) Schilz, J.; Riffel, M.; Pixius, K.; Meyer, H. J. Synthesis of Thermoelectric Materials by Mechanical Alloying in Planetary Ball Mills. *Powder Technol.* **1999**, *105*, 149−154.
(5) Kulbachinskii, V. A.; Kytin, V. G.; Zinoviev, D. A.; Maslov, N. V.; Singha, P.; Das, S.; Banerjee, A. Thermoelectric Properties of Sb2Te3-Based Nanocomposites with Graphite. *Semiconductors* **2019**, *53*, 638−640.
(6) Ballikaya, S.; Chi, H.; Salvador, J. R.; Uher, C. Thermoelectric Properties of Ag-Doped Cu_2Se and Cu_2Te. *J. Mater. Chem. A* **2013**, *1*, 12478−12484.
(7) Zhao, K.; Blichfeld, A. B.; Chen, H.; Song, Q.; Zhang, T.; Zhu, C.; Ren, D.; Hanus, R.; Qiu, P.; Iversen, B. B.; Xu, F.; Snyder, G. J.; Shi, X.; Chen, L. Enhanced Thermoelectric Performance through Tuning Bonding Energy in $Cu_2Se_{1-X}S_x$ Liquid-like Materials. *Chem. Mater.* **2017**, *29*, 6367−6377.
(8) Bailey, T. P.; Hui, S.; Xie, H.; Olvera, A.; Poudeu, P. F. P.; Tang, X.; Uher, C. Enhanced ZT and Attempts to Chemically Stabilize Cu_2Se via Sn Doping. *J. Mater. Chem. A* **2016**, *4*, 17225−17235.
(9) Zhao, K.; Blichfeld, A. B.; Eikeland, E.; Qiu, P.; Ren, D.; Iversen, B. B.; Shi, X.; Chen, L. Extremely Low Thermal Conductivity and High Thermoelectric Performance in Liquid-like $Cu_2Se_{1-: X}S_x$ Polymorphic Materials. *J. Mater. Chem. A* **2017**, *5*, 18148−18156.
(10) Zhong, B.; Zhang, Y.; Li, W.; Chen, Z.; Cui, J.; Xie, Y.; Hao, Q.; He, Q.; et al. High Superionic Conduction Arising from Aligned Large Lamellae and Large Figure of Merit in Bulk $Cu_{1.94}Al_{0.02}Se$. *Appl. Phys. Lett.* **2014**, *105*, No. 123902.
(11) Peng, P.; Gong, Z. N.; Liu, F. S.; Huang, M. J.; Ao, W. Q.; Li, Y.; Li, J. Q. Structure and Thermoelectric Performance of β-Cu_2Se Doped with Fe, Ni, Mn, In, Zn or Sm. *Intermetallics* **2016**, *75*, 72−78.
(12) Nieroda, P.; Kusior, A.; Leszczyński, J.; Rutkowski, P.; Koleżyński, A. Thermoelectric Properties of Cu_2Se Synthesized by Hydrothermal Method and Densified by SPS Technique. *Materials* **2021**, *14*, No. 3650.
(13) Mallick, M. M.; Georg Rösch, A.; Franke, L.; Ahmed, S.; Gall, A.; Geßwein, H.; Aghassi, J.; Lemmer, U. High-Performance Ag−Se-Based n-Type Printed Thermoelectric Materials for High Power Density Folded Generators. *ACS Appl. Mater. Interfaces* **2020**, *12*, 19655−19663.
(14) Rösch, A. G.; Gall, A.; Aslan, S.; Hecht, M.; Franke, L.; Mallick, M. M.; Penth, L.; Bahro, D.; Friderich, D.; Lemmer, U. Fully Printed Origami Thermoelectric Generators for Energy-Harvesting. *npj Flexible Electron.* **2021**, *5*, No. 3.
(15) Scimeca, M. R.; Yang, F.; Zaia, E.; Chen, N.; Zhao, P.; Gordon, M. P.; Forster, J. D.; Liu, Y. S.; Guo, J.; Urban, J. J.; Sahu, A. Rapid Stoichiometry Control in Cu_2Se Thin Films for Room-Temperature Power Factor Improvement. *ACS Appl. Energy Mater.* **2019**, *2*, 1517−1525.
(16) Pammi, S. V. N.; Jella, V.; Choi, J. S.; Yoon, S. G. Enhanced Thermoelectric Properties of Flexible $Cu_{2-x}Se$ ($x \geq 0.25$) NW/Polyvinylidene Fluoride Composite Films Fabricated via Simple Mechanical Pressing. *J. Mater. Chem. C* **2017**, *5*, 763−769.
(17) Lu, Y.; Ding, Y.; Qiu, Y.; Cai, K.; Yao, Q.; Song, H.; Tong, L.; He, J.; Chen, L. Good Performance and Flexible PEDOT:PSS/Cu_2Se Nanowire Thermoelectric Composite Films. *ACS Appl. Mater. Interfaces* **2019**, *11*, 12819−12829.
(18) Lu, Y.; Li, X.; Cai, K.; Gao, M.; Zhao, W.; He, J.; Wei, P. Enhanced-Performance PEDOT:PSS/Cu_2Se-Based Composite Films for Wearable Thermoelectric Power Generators. *ACS Appl. Mater. Interfaces* **2021**, *13*, 631−638.
(19) Mallick, M. M.; Franke, L.; Rösch, A. G.; Ahmad, S.; Geßwein, H.; Eggeler, Y. M.; Rohde, M.; Lemmer, U. Realizing High Thermoelectric Performance of Bi-Sb-Te-Based Printed Films through Grain Interface Modification by an In Situ-Grown β-$Cu_{2-\delta}Se$ Phase. *ACS Appl. Mater. Interfaces* **2021**, *13*, 61386−61395.
(20) Mallick, M. M.; Sarbajna, A.; Rösch, A. G.; Franke, L.; Geßwein, H.; Eggeler, Y. M.; Lemmer, U. Ultra-Flexible β-$Cu_{2-\delta}Se$-Based p-Type Printed Thermoelectric Films. *Appl. Mater. Today* **2021**, *44*, No. 101269.
(21) Kim, M.; Park, D.; Kim, J. Thermoelectric Generator Using Polyaniline-Coated Sb_2Se_3/β-Cu_2Se Flexible Thermoelectric Films. *Polymers* **2021**, *13*, No. 1518.
(22) Mallick, M. M.; Rösch, A. G.; Franke, L.; Gall, A.; Ahmad, S.; Geßwein, H.; Mazilkin, A.; Kübel, C.; Lemmer, U. New Frontier in Printed Thermoelectrics: Formation of β-Ag_2Se through Thermally Stimulated Dissociative Adsorption Leads to High: ZT. *J. Mater. Chem. A* **2020**, *8*, 16366−16375.
(23) Mallick, M.; Franke, L.; Rösch, A. G.; Lemmer, U. Shape-Versatile 3D Thermoelectric Generators by Additive Manufacturing. *ACS Energy Lett.* **2021**, *6*, 85−91.
(24) Rösch, A. G.; Giunta, F.; Mallick, M. M.; Franke, L.; Gall, A.; Aghassi-Hagmann, J.; Schmalian, J.; Lemmer, U. Improved Electrical, Thermal, and Thermoelectric Properties Through Sample-to-Sample Fluctuations in Near-Percolation Threshold Composite Materials. *Adv. Theory Simul.* **2021**, *4*, No. 2000284.
(25) Mallick, M. M.; Vitta, S. Thermophysical and Magnetic Properties of P- and n-Type Ti-Ni-Sn Based Half-Heusler Alloys. *J. Alloys Compd.* **2017**, *710*, 191−198.
(26) Singh, H.; Bernabe, J.; Chern, J.; Nath, M. Copper Selenide as Multifunctional Non-Enzymatic Glucose and Dopamine Sensor. *J. Mater. Res.* **2021**, *36*, 1413−1424.
(27) Khusayfan, N. M.; Khanfar, H. K. Structural and Optical Properties of Cu_2Se/Yb/Cu_2Se Thin Films. *Results Phys.* **2019**, *12*, 645−651.
(28) Maiti, S.; Maiti, S.; Khan, A. H.; Wolf, A.; Dorfs, D.; Moreels, I.; Schreiber, F.; Scheele, M. Dye-Sensitized Ternary Copper Chalcogenide Nanocrystals: Optoelectronic Properties, Air Stability, and Photosensitivity. *Chem. Mater.* **2019**, *31*, 2443−2449.

https://doi.org/10.1021/acsomega.2c00412
ACS Omega 2022, 7, 10695−10700